ARTICLE

OBC
www.rsc.org/obc

Exploring the boundaries of a light-driven molecular motor design: new sterically overcrowded alkenes with preferred direction of rotation †

Richard A. van Delden, Matthijs K. J. ter Wiel, Harmen de Jong, Auke Meetsma and Ben L. Feringa *

Department of Organic and Molecular Inorganic Chemistry Stratingh Institute, University of Groningen, Nijenborgh 4, 9747 AG Groningen, The Netherlands. E-mail: feringa@chem.rug.nl

Received 13th February 2004, Accepted 19th March 2004
First published as an Advance Article on the web 26th April 2004

Insight in the steric and electronic parameters governing isomerization processes in artificial molecular motors is essential in order to design more advanced motor systems. A subtle balance of steric parameters and the combination of helical and central chirality are key features of light-driven unidirectional rotary molecular motors constructed so far. In an approach to decrease the steric hindrance around the central olefinic bond (rotary axis) and thereby lowering the energy barrier for helix inversion resulting in an increased rotation rate, the boundaries of our molecular motor design are explored. In a new design of a light-driven molecular motor based on a sterically overcrowded alkene the methyl substituent adjacent to the stereogenic center, which is responsible for the control of the direction of rotation, is shifted one position away from the fjord region of the molecule compared to the second-generation motor systems. In contrast to previously developed light-driven molecular motors, there is a preference for the methyl substituent to adopt a pseudo-equatorial orientation. Nevertheless, this new type of motor is capable of functioning as a rotary molecular motor, albeit not with full unidirectionality. Under the combined influence of light and heat, there is a preferred clockwise rotation of one half of the molecule. Surprisingly, the effect of shifting the methyl substituent on the energy barrier for helix inversion is small and even a slight increase in the barrier is observed.

Introduction

The bottom-up construction of essential components for the future toolbox of nanotechnology offers a major challenge for scientists crossing traditional borders between chemistry, physics and molecular biology.[1] Recently reported molecular mechanical devices,[2] in which controlled motion at the molecular level is a key feature, include switches,[3] brakes,[4] gears,[5] turnstiles,[6] scissors,[7] rotating modules,[8] and muscles.[9] In pursuit of true molecular motors,[10] Nature's diversity of fascinating rotary and linear molecular motors[11] offer a major source of inspiration. Molecular machines[1c,12] based on redox-driven metal ion translocation[13] and molecular shuttles based on (pseudo-)rotaxane or catenane systems are prominent examples of artificial systems that have been developed.[14] In 1999, the first examples of unidirectionally rotating molecular motors derived from simple organic molecules, driven by chemical[15] or light energy[16] were reported.[17] The first light-driven unidirectional molecular motor was based on a sterically overcrowded alkene. Chiral sterically overcrowded alkenes have proven to be versatile systems for the development of photoactive molecular devices. They do not only form the basis for light-driven molecular motors,[18] but also for chiroptical molecular switches,[19] which have, for example, been used as chiral phototriggers of liquid crystal phase transitions.[20,21] Essential features of these systems are an intrinsically chiral helical shape and a photoisomerizable central carbon–carbon double bond.

In the first light-driven unidirectional molecular motor based on a sterically overcrowded alkene (Fig. 1A), intramolecular rotation is driven by light energy and the directionality of rotation is fully controlled by the subtle interplay of two stereogenic centers and the intrinsic helical conformation. One full rotation involves two energetically uphill photoisomerizations (*hν* in Fig. 1) and two energetically downhill thermal helix inversion steps (Δ in Fig. 1). The key feature of this concept is the energetic preference for the methyl substituents next to the stereogenic centers to adopt an axial orientation, which is less sterically demanding and energetically favorable. The two photoisomerization steps force the methyl substituents into an unfavorable diequatorial orientation. Subsequent energetically downhill thermal helix inversion steps restore the diaxial conformation, ensuring the unidirectionality of the rotary process.

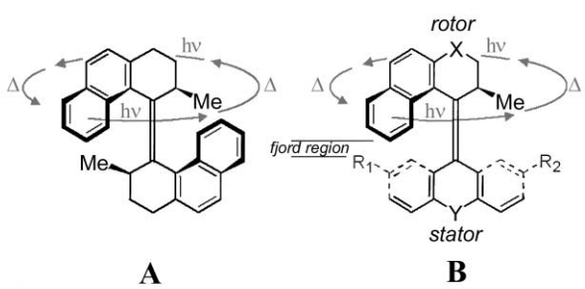

Fig. 1 First (A) and second (B) generation molecular motors: unidirectional rotation in a four step (two thermal (Δ) and two photochemical (*hν*) steps) rotary cycle.

The first generation molecular motor was used to drive color changes in a liquid crystal matrix, which represents the first example of a synthetic molecular motor performing actual work.[22,23] Nevertheless, this system showed some shortcomings for further applications. The most important is that a substantial amount of thermal energy is required to overcome the barriers of the thermal helix inversion steps to induce continuous rotary motion. In order to be able to tune the speed of the rotary motion a second-generation molecular motor (Fig. 1B) was developed.[24] This second-generation motor consists of two separate entities, a so-called rotor part, which governs the

† Electronic supplementary information (ESI) available: a table to convert the labels in the X-ray structure used in the paper and the cif-files. See http://www.rsc.org/suppdata/ob/b4/b402222j/

DOI: 10.1039/b402222j

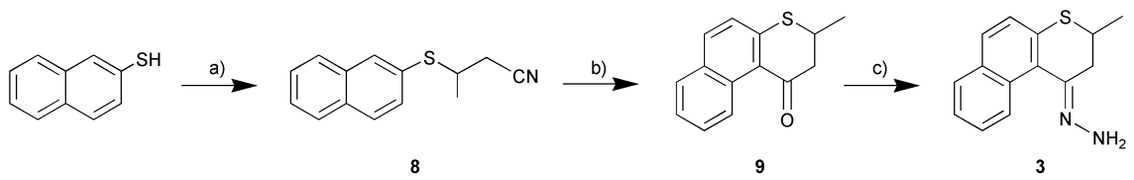

8 9 3

Scheme 1 Synthesis of hydrazone upper half: a) crotononitrile, piperidine, Triton B/MeOH, Δ, 91%; b) PPA, 110 °C, 86%; c) $H_2NNH_2 \cdot H_2O$, EtOH, Δ, 74%.

unidirectional rotation, and a stator part. Both parts can be functionalized and modified in order to tune the properties of the molecular motor. Essentially, this second-generation motor works in the same way as the first-generation motor. Unidirectional rotation is achieved by the combined action of two photo-induced isomerizations and two thermal helix inversion steps. The unidirectional rotation is now controlled by the subtle interplay of a single stereogenic center in the rotor half of the molecule with the intrinsic chiral structure around the central olefinic bond. Again, the energetic preference for the methyl substituent in the rotor half of the molecule to adopt a (pseudo-)axial orientation was shown to be the key feature. From ongoing research on sterically overcrowded alkenes it was already evident that steric hindrance in the so-called fjord region of the system (Fig. 1) is the major contributor to the height of the helix inversion barriers.

With the design of the second-generation light-driven molecular motor it was possible to reduce the energy barriers significantly by changing the bridging atoms X and Y, which enhances the speed of rotation by a factor >300, resulting in a motor capable of functioning at ambient temperatures.[25] The half-life of the thermal helix inversion steps for the fastest molecular motor is still 2400 s at room temperature. The major challenge therefore remains the lowering of the barriers for the rate determining thermal steps. In a first approach, the size of the upper arene part of the molecule was reduced (Fig. 2A). Surprisingly, although this system still functions as a molecular motor, after elimination of one arene ring in the upper part, the inversion barriers are increased and the rotation is slowed down.[26] This remarkable effect was attributed to a higher ground state stability of this molecule relative to the transition state. It is evident that these energy barriers are not only influenced by steric effects but also ground-state energy plays a significant and, in this specific case, decisive role.

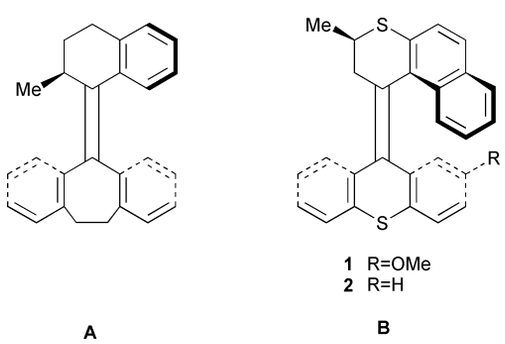

Fig. 2 New molecular motor designs with decreased steric hindrance in the fjord region due to (A) elimination of arene unit in rotor part and (B) shift of methyl-group in rotor part.

Besides the aromatic part of the rotor half, the methyl substituent has a substantial effect on the steric hindrance around the fjord region. This substituent basically governs the directionality of molecular rotation but also contributes to the energy barriers for helix inversion. Here we report a new type of molecular motor (structures **1** and **2**) where the methyl group is shifted one position away from the fjord region (Fig. 2B). The objective of this approach was to decrease the steric hindrance around the fjord region and thereby lowering the energy barrier for helix inversion. The major questions are whether this new system can still function as a molecular motor and if the speed of rotation is increased. Since the steric hindrance between upper and lower half is responsible both for the energy difference between stable and unstable forms, essential for functioning of the molecular motors (unidirectional rotation), as well as for the energy barriers for helix inversion (stagnating smooth continuous rotation) the bulk around the fjord region should be balanced carefully. With the newly designed sterically overcrowded alkenes **1** and **2** we explore the boundaries of our molecular motor design.

Results and discussion

Synthesis

Compounds **1** and **2** were synthesized using a convergent route, constructing the sterically demanding central olefinic bond in a late stage of the synthesis by coupling the upper half hydrazone **3** (Scheme 1) and lower half thioketone **4** or **5** (Scheme 2). The racemic upper half hydrazone **3** was prepared starting from 2-naphthalenethiol (Scheme 1). A Michael-addition to crotononitrile afforded 3-(2-naphthylsulfanyl)butanenitrile **8** in 91% yield and subsequent ring-closure *via* an intramolecular Friedel–Crafts acylation provided ketone **9** in 86% yield. Reaction with hydrazine monohydrate in ethanol gave the desired hydrazone **3** in 74% yield. The synthesis of thioketones **4** and **5** has been reported elsewhere.[25]

Coupling of the upper and lower half was achieved by the Barton–Kellogg method (Scheme 2).[27] First, reaction of **3** with Ag_2O gave the upper half diazo-compound which was allowed to react *in situ* with the lower half thioketones **4** and **5** *via* a 1,3-dipolar cycloaddition. This resulted in the formation of a five-membered thiadiazoline intermediate, which eliminated nitrogen to form the episulfides **6** and **7**. After extrusion of sulfur under the influence of PPh_3, the desired sterically hindered alkenes **1** and **2** were obtained as a mixture of diastereoisomers (*vide infra*) in 56% and 52% yield, respectively.

Resolution and stereochemistry

Compound **1** can exist in a *trans*- (**1a**) and *cis*- (**1b**) geometry and two chiral entities (the stereogenic center (*S* or *R*) and the intrinsic helical chirality (*P* or *M*)) give rise to eight diastereoisomers, four diastereoisomers for both *trans*-**1a** and *cis*-**1b** (Fig. 3). Since, in the synthesis, the coupling was performed with a racemic upper half, all eight isomers were obtained. As a consequence of the helical conformation, in case of the (3′*S*)-(*P*)- and (3′*R*)-(*M*)-isomers, the upper half methyl substituent adopts a pseudo-equatorial orientation. In case of the (3′*R*)-(*P*)- and (3′*S*)-(*M*)-isomers, the upper half methyl substituent adopts a pseudo-axial orientation (these isomers are denoted with a prime: **1′a** and **1′b**). For compound **1**, the *trans*- and *cis*-isomers could clearly be distinguished by ^{1}H NMR. A characteristic signal is the singlet of the methoxy substituent, which for *trans*-**1a** has a chemical shift of δ 3.87 ppm and for *cis*-**1b** has a chemical shift of 3.04 ppm, due to shielding of the methoxy substituent by the arene upper half in the latter case (for full NMR details see Experimental section). For both the *cis* and *trans* isomers, a mixture of all four possible diastereoisomers, composed of a major—most stable—pair of enantiomers with pseudo-equatorial methyl substituents

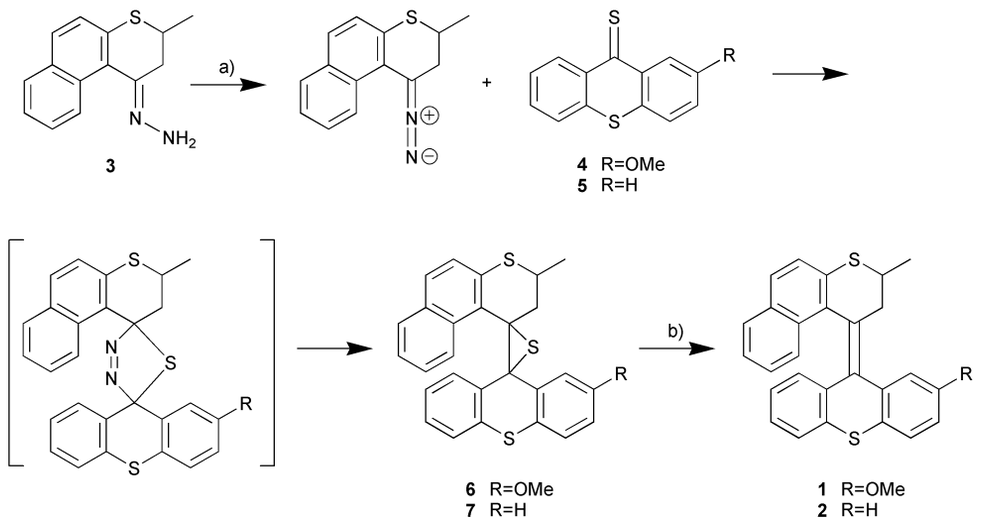

Scheme 2 Coupling of upper and lower half of sterically overcrowded alkenes *via* a diazo-thioketone coupling: a) Ag_2O, KOH/MeOH, CH_2Cl_2, −30 °C ⟶ rt, **6** (51%), **7** (53%); b) PPh_3, *p*-xylene, Δ, **1** (56%), **2** (52%).

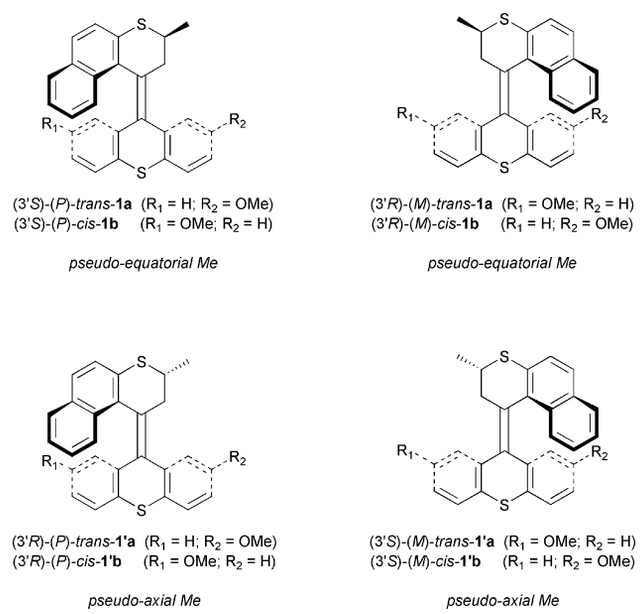

Fig. 3 All eight possible stereoisomers of sterically overcrowded alkene **1**.

(**1a/1b**) and a minor—less stable—pair with pseudo-axial methyl substituents (**1′a/1′b**) in a 10 : 1 ratio, was obtained from the synthesis.

For both the *cis*- and the *trans*-isomers, the different stereoisomers were analyzed by CD spectroscopy, where (*M*)- and (*P*)-helicity could be assigned by comparison with related sterically overcrowded alkenes.[25] The configuration at the stereogenic center could be assigned considering the energetic preference for a pseudo-equatorial methyl substituent (see X-ray structure *vide infra*). The *cis*- and *trans*-isomers could be separated by preferred crystallization and, for both *cis*- and *trans*-**1**, two of the four diastereoisomers could be obtained enantiomerically pure by chiral HPLC. For *trans*-**1**, using a Chiralcel OD column and *n*-heptane : 2-propanol 99 : 1 as the eluent, the first eluted fraction contained both (*M*)-enantiomers: (3′*R*)-(*M*)-*trans*-**1a** and (3′*S*)-(*M*)-*trans*-**1′a** in an approximately 10 : 1 ratio, again reflecting their relative stability. The second fraction contained pure (3′*S*)-(*P*)-*trans*-**1a** (CD (chloroform): λ_{max} (Δε) 254 (−37.9), 281 (+136.5), 323 (−14.6), 356 (−20.9)) and the third fraction consisted of pure (3′*R*)-(*P*)-*trans*-**1′a** (CD (chloroform): λ_{max} (Δε) 256 (−14.2), 281 (+114.8), 320 (−19.7), 343 (−18.9)). Using the same conditions for *cis*-**1** the elution pattern was similar: the first eluted fraction consisted of (3′*R*)-(*M*)-*cis*-**1b** and (3′*S*)-(*M*)-*cis*-**1′b** again in a 10 : 1 ratio. The second fraction consisted of pure (3′*S*)-(*P*)-*cis*-**1b** (CD (chloroform): λ_{max} (Δε) 254 (−66.3), 280 (+115.7), 359 (−16.8)) and the third fraction consisted of pure (3′*R*)-(*P*)-*cis*-**1′b** (CD (chloroform): λ_{max} (Δε) 255 (−29.9), 279 (+110.2), 316 (−10.7), 348 (−14.2)).

Compound **2**, due to a symmetric lower half, is obtained as a mixture of only 2 pairs of enantiomers (Fig. 4), again in a ratio of approximately 10 : 1. Assignment of helical conformation and the configuration at the stereogenic center was performed as described above for **1**. The energetically preferred major pair of enantiomers was assigned (3′*S*)-(*P*)-**2** and (3′*R*)-(*M*)-**2**. The disfavored minor pair of enantiomers, again denoted with a prime, are (3′*S*)-(*M*)-**2′** and (3′*R*)-(*P*)-**2′**. In full accordance with the results obtained for compound **1**, there is an energetic preference for a pseudo-equatorial orientation of the methyl substituent. Two of these four diastereoisomers could be obtained pure by chiral HPLC. The elution order and conditions for both forms are identical to those of compound **1**. Employing a Chiralcel OD column and *n*-heptane : 2-propanol 99 : 1 as the eluent, the first eluted fraction contained both (3′*R*)-(*M*)-**2** and (3′*S*)-(*M*)-**2′**, the second fraction consisted of enantiomerically pure (3′*S*)-(*P*)-**2** (CD (chloroform): λ_{max} (Δε) 255 (−25.2), 280 (+105.8), 322 (−9.4), 353 (−16.8)) and the

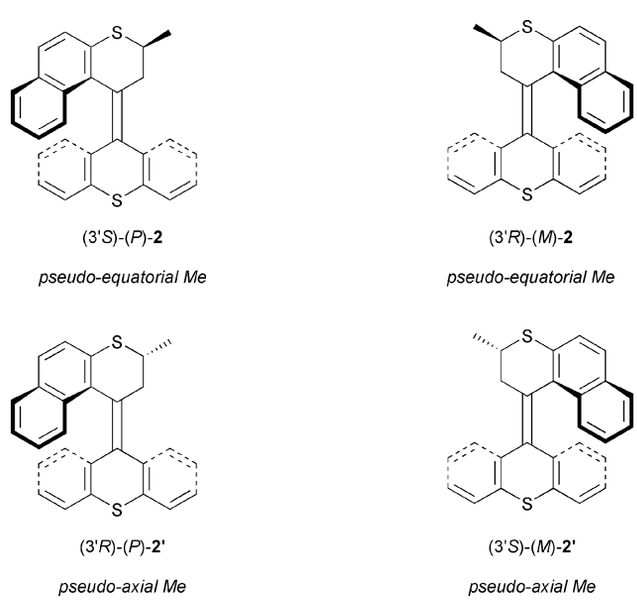

Fig. 4 The four possible stereoisomers of sterically overcrowded alkene **2**

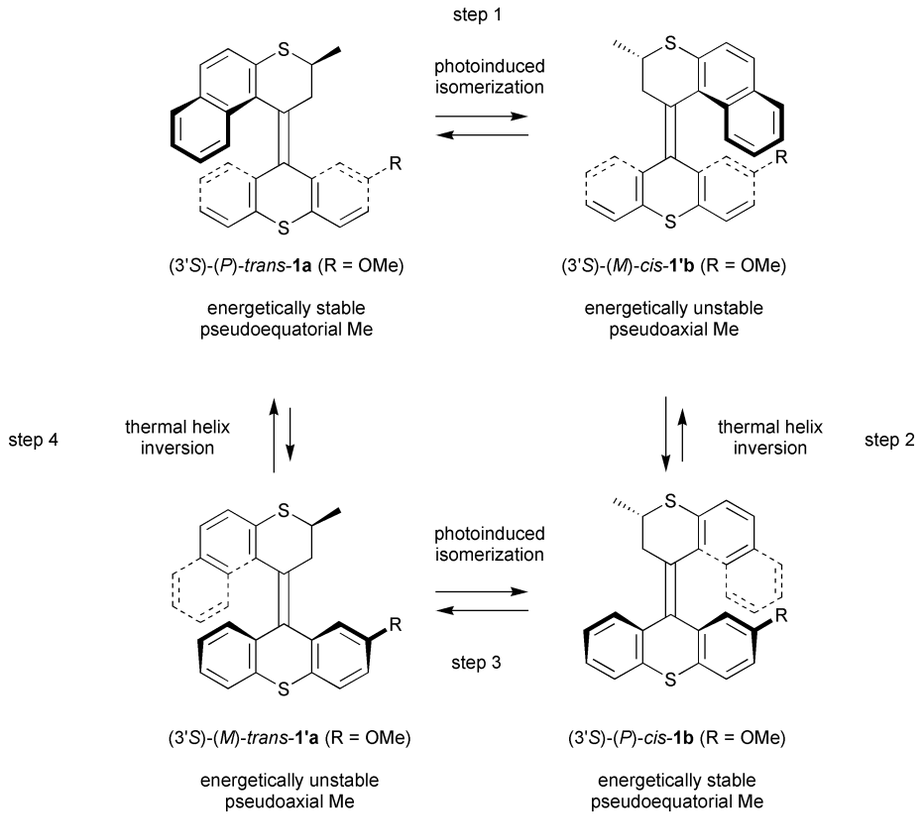

Scheme 3 Photochemical and thermal isomerization steps of newly designed sterically overcrowded alkene **1**.

third fraction contained enantiomerically pure (3′*R*)-(*P*)-**2**′ (CD (chloroform): λ_{max} ($\Delta\varepsilon$) 255 (−12.7), 279 (+103.7), 317 (−16.4), 345 (+15.5)).

X-Ray analysis of unsubstituted motor 2. In order to confirm the structure of the energetically favored isomers of these new systems, a single crystal of the major isomer of racemic **2** was subjected to X-ray analysis (Fig. 5). The racemic crystal was found to be monoclinic: space group $P2_1/n$.[28] The geometry of (3′*S*)-(*P*)-**2** (the enantiomer depicted) in the solid state is characterized as follows: central double bond, C(1′)–C(9) = 1.349 Å; bond angles around central double bond, C(8a)–C(9)–C(9a) = 113.0°, C(8a)–C(9)–C(1′) = 122.4°, C(9a)–C(9)–C(1′) = 124.5° (total angle around C(9) is 359.9°), C(10′b)–C(1′)–C(2′) = 111.0°, C(10′b)–C(1′)–C(9) = 124.3°, C(2′)–C(1′)–C(9) = 124.5° (total angle around C(1′) is 359.8°); the dihedral angle between the naphthalene plane of the upper part and the central double bond, C(10′a)–C(10′b)–C(1′)–C(9) = 61.4°; dihedral angles between the thioxanthene arene moieties of the lower part and the central double bond, C(1′)–C(9)–C(9a)–C(1) = −50.6°, C(1′)–C(9)–C(8a)–C(8) = 49.9°; dihedral angles at the central double bond, C(10′b)–C(1′)–C(9)–C(8a) = 3.7°, C(2′)–C(1′)–C(9)–C(9a) = 8.3° (average value is 6.0°), C(8a)–C(9)–C(1′)–C(2′) = −172.5°, C(9a)–C(9)–C(1′)–C(10′b) = −175.5° (average value is 174.56°). The central double bond is therefore slightly twisted, although each sp^2 carbon of the central double bond remains essentially planar. The lower thioxanthene part of the molecule adopts a folded structure to diminish the steric strain around the central double bond and, together with the pseudo-boat conformation of the thiopyran ring of the upper part, is responsible for the helical shape of the entire molecule.

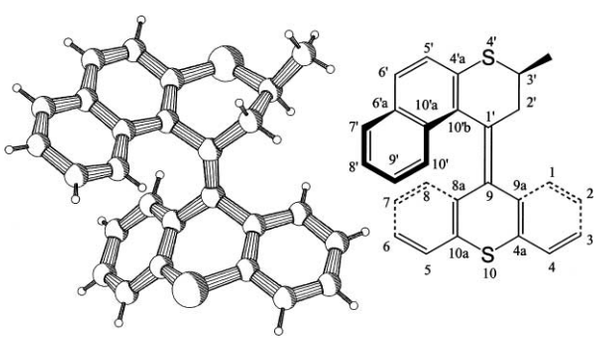

Fig. 5 PLUTO drawing of stable isomer of **2**.

Although the absolute configuration was not determined, it was confirmed that the (3′*S*)-enantiomer showed a preferred (*P*)-helicity while the (3′*R*)-enantiomer showed a preferred (*M*)-helicity. Due to strong distortion (pseudo-boat conformation) of the upper half thiopyran ring and the presence of the adjacent aromatic moiety and the neighboring sulfur atom, it is difficult to unequivocally assign the orientation of the 3′-methyl substituent as being equatorial or axial. However, the relative position with respect to the protons at the 2′-position (where clear distinction can be made between pseudo-axial and pseudo-equatorial orientation), shows that, in the energetically most favorable state, the 3′-methyl adopts a pseudo-equatorial position. This conformation is in contrast to that of all reported second-generation motors[25] for which the methyl substituent adopts an energetically favorable axial orientation. In both types of compounds, however, the methyl substituent has a preferred *anti*-orientation with respect to the aromatic lower half as is clearly seen in the X-ray structure of **2**. AM1 calculations using MOPAC93[29] confirm the observed preference for the methyl substituent to adopt a pseudo-equatorial orientation. For compound **1**, energy differences of 8.04 kJ mol^{-1} between *trans*-**1a** and *trans*-**1′a** and 8.12 kJ mol^{-1} between *cis*-**1b** and *cis*-**1′b**, both in favor of a pseudo-equatorial methyl substituent, were calculated. Analogously, for **2** an energy difference of 8.19 kJ mol^{-1} between **2** and **2**′ was calculated.

Isomerization pathways of 1. We envisioned compound **1** to function as a four state rotating motor as shown in Scheme 3. Starting from the more stable (3′*S*)-(*P*)-*trans*-isomer **1a**, with a pseudo-equatorially oriented methyl group, a photoinduced

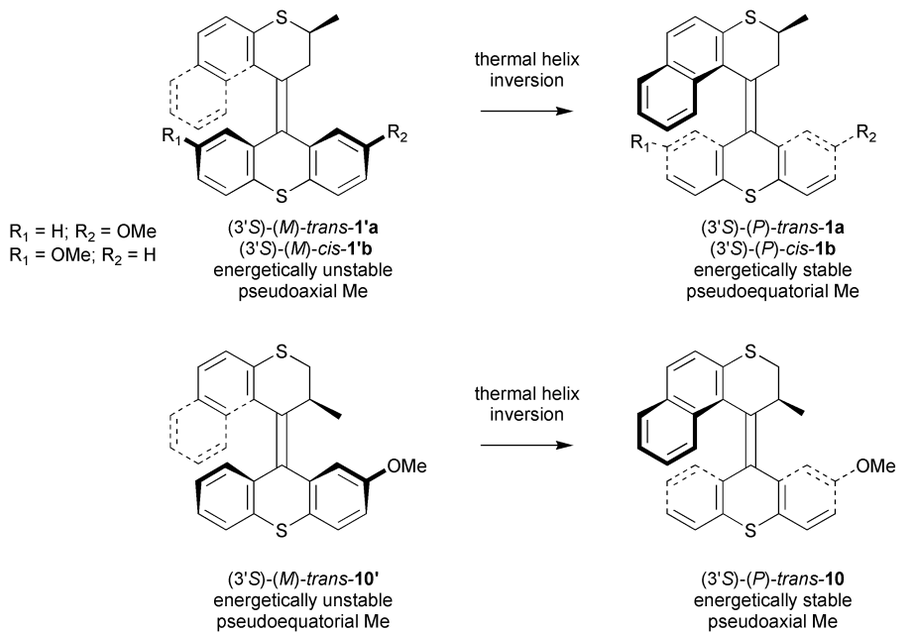

Scheme 4 Thermal helix inversion of the new motor system **1** compared to second-generation motor **10**.

trans–cis isomerization would yield a photostationary state consisting of *trans*-**1a** and less stable *cis*-**1′b** (step 1). Subsequent heating would lead to relaxation of the molecule by helix inversion of *cis*-**1′b** to yield the more stable *cis*-form *cis*-**1b** (step 2). A second energetically uphill photoisomerization will give *trans*-**1′a** (step 3) and a second energetically downhill thermal helix inversion (step 4) completes a full 360° rotation, resulting again in the formation of the *trans*-**1a** isomer.

The key aspect of this system functioning as a unidirectional molecular motor is the energy difference between the isomers with pseudo-equatorial and pseudo-axial methyl substituents, which governs the direction of rotation. In the case of our second-generation motors (exemplified by **10** in Scheme 4), this energy difference (in this case in favor of a pseudo-axially oriented methyl substituent) was sufficient to induce full unidirectionality. For **1**, the preferred pseudo-equatorial orientation of the methyl substituents might still allow 360° rotation driven by light, but considering the energy differences calculated for the stable and unstable isomers this four step rotary cycle might not be fully unidirectional. A calculation of the Boltzmann distribution of stable and unstable forms at room temperature using the smallest determined energy difference (8.04 kJ mol^{-1} for *trans*-**1a**, *vide supra*) shows that about 3.5% of unstable form will be present at equilibrium. At elevated temperatures more and more of the unstable form will be present (about 5% at 55 °C). This means that if the appropriate temperature allows thermal helix inversion, according to these calculations this helix inversion will take place in both directions to a considerable extent. For comparison: for the second-generation motor bearing a methoxy-substituent **8**, an energy difference between stable and unstable diastereoisomers of 19.46 kJ mol^{-1} was calculated for both the *cis*- and *trans*-isomers, employing the same calculation method. On the basis of this energy difference the population of the unstable isomer is negligible after thermal helix inversion (0.002% according to the Boltzmann distribution). This is in agreement with the quantitative thermal conversion of the second-generation motors observed by ^{1}H NMR spectroscopy.[25]

The photochemical and thermal steps of the proposed four state intramolecular rotation were examined stepwise, starting from stable isomers (3′*S*)-(*P*)-*trans*-**1a** and (3′*S*)-(*P*)-*cis*-**1b** using UV-Vis, CD and NMR spectroscopy in chloroform ($CHCl_3$ and $CDCl_3$) solution. The UV-Vis and CD absorption spectra of all (3′*S*)-isomers in chloroform are shown in Fig. 6.

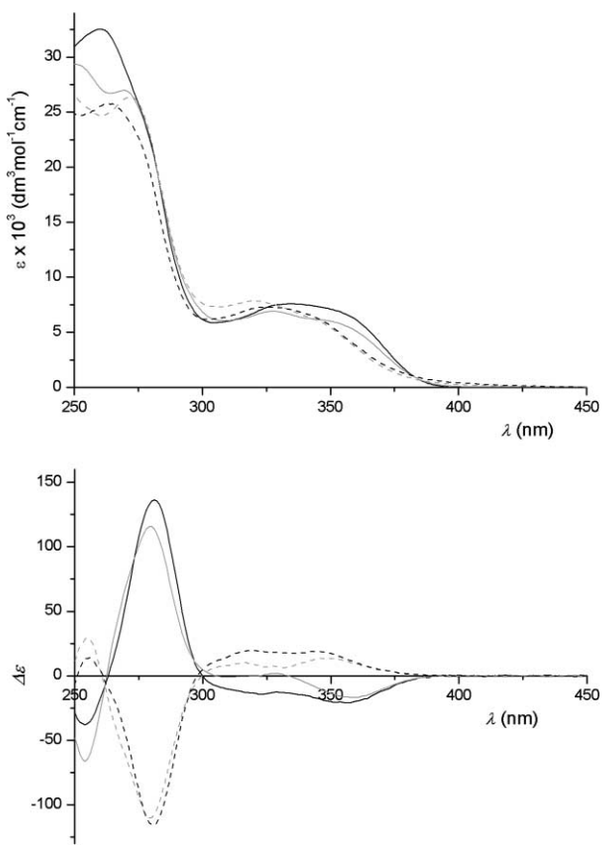

Fig. 6 UV (top) and CD (bottom) characteristics of **1a** and **1b** ((3′*S*)-(*P*)-*trans*-**1a**: —; (3′*S*)-(*M*)-*cis*-**1′b**: ----; (3′*S*)-(*P*)-*cis*-**1b**: —; (3′*S*)-(*M*)-*trans*-**1′a**: ----) in chloroform.

Photoisomerization of (3′*S*)-(*P*)-*trans*-1a. A sample of enantiomerically pure (3′*S*)-(*P*)-*trans*-**1a** in chloroform was irradiated with light of $\lambda \geq 280$ nm (Pyrex filter). A clear decrease in the major CD band from $\Delta\varepsilon$ −136.5 (λ_{max} = 281 nm) to $\Delta\varepsilon$ −36.2 (λ_{max} = 278 nm) was observed but a full reversal of the CD spectrum expected for the formation of the pseudo-enantiomeric (3′*S*)-(*M*)-*cis*-**1′b** form did not occur. ^{1}H NMR analysis clearly showed the formation of the *cis*-isomer, the characteristic absorption of the methoxy-protons shifted upfield from δ 3.87 to 3.04 ppm due to shielding of the methoxy-proton by the upper arene part of the molecule in case of

the *cis*-isomer. The doublet signal of the protons of the upper half methyl group was shifted from δ 1.61 to 1.74 ppm indicating the conformational change from a pseudo-equatorial to a pseudo-axial orientation. In the aromatic region, three signals, clearly belonging to (3′*S*)-(*M*)-*cis*-**1′b**, appeared at δ 5.86 (bs, 1H), 6.26 (dd, J = 8.8, 3.0 Hz, 1H) and 7.79 ppm (d, J = 7.3 Hz, 1H) (all other signals overlap). ^{1}H NMR analysis after irradiation at $\lambda \geq 280$ nm indicated a photostationary state consisting of 69.4% of the anticipated (3′*S*)-(*M*)-*cis*-**1′b** and 30.6% of the initial (3′*S*)-(*P*)-*trans*-**1a** isomer. This photostationary ratio is partly governed by the ratio of extinction coefficients at the wavelength used in the irradiation experiments. Closer investigation of the UV-Vis absorption spectra of the two forms indicated that the maximum in the ratio of the extinction coefficients was found at 365 nm. Prolonged irradiation using an interference filter at this wavelength, however, had no effect on the photoequilibrium. From the isomer ratio, together with the CD data for pure (3′*S*)-(*P*)-*trans*-**1a** and the CD data of the photostationary mixture, the CD spectrum of pure (3′*S*)-(*M*)-*cis*-**1′b** could be calculated (Fig. 6). From the CD spectra it is clearly seen that (3′*S*)-(*P*)-*trans*-**1a** and (3′*S*)-(*M*)-*cis*-**1′b** are pseudoenantiomers.

To induce the second step in the rotary cycle the sample was heated at 55 °C and the change in the CD band at 285 nm was monitored with time (Fig. 7). Detailed analysis of the sample after heating revealed that through thermal helix inversion indeed the (3′*S*)-(*M*)-*cis*-**1′b** isomer was converted to the more stable (3′*S*)-(*P*)-*cis*-**1b** with a pseudo-equatorial methyl group. However, only 94.0% of (3′*S*)-(*P*)-*cis*-**1b** was observed at thermal equilibrium, the remaining 6.0% was still the initial (3′*S*)-(*M*)-*cis*-**1′b** isomer. This indicates substantial stability of the (3′*S*)-(*M*)-*cis*-**1′b** isomer at elevated temperatures and therefore this thermal helix inversion is a reversible process. At 55 °C, simultaneously, in an energetically uphill process, the remaining (3′*S*)-(*P*)-*trans*-**1a** was converted to the less stable (3′*S*)-(*M*)-*trans*-**1′a** isomer to a substantial extent (16.6%). Also in the case of the *trans*-isomer, the less stable (3′*S*)-(*M*)-*trans*-**1′a** isomer has sufficient stability to make the thermal helix inversion an equilibrium process under these conditions. Both thermal processes together resulted in a complicated mixture of all four isomers (as determined by ^{1}H NMR and HPLC) but the major CD band again increased from $\Delta\varepsilon$ −36.2 (λ_{max} = 278 nm) to $\Delta\varepsilon$ +99.6 (λ_{max} = 280 nm) because there is a thermal preference for the (*P*)-isomers of *cis*- and *trans*-**1** due to the (3′*S*)-configuration at the stereogenic center.

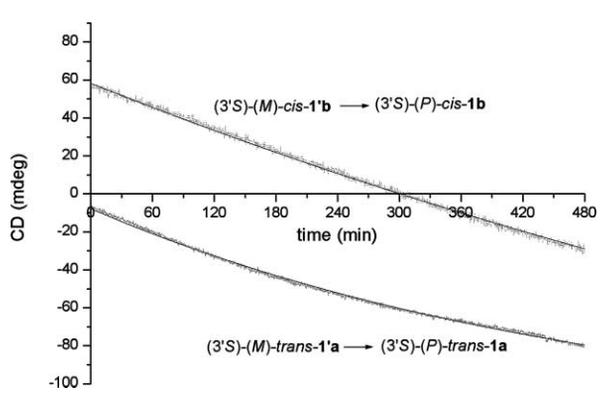

Fig. 7 Experimental curves (gray) and fit (black) for two separate thermal helix inversion steps followed by CD spectroscopy. Although both thermal processes simultaneously take place, the major processes are given.

A separate sample of the stable enantiomerically pure (3′*S*)-(*P*)-*cis*-**1b** isomer showed a distinct strong positive CD absorption ($\Delta\varepsilon$ +115.7) at 280 nm (Fig. 6) and irradiation of this sample yielded a photostationary state consisting of 48.9% of (3′*S*)-(*P*)-*cis*-**1b** and 51.1% of (3′*S*)-(*M*)-*trans*-**1′a** (^{1}H NMR). Analogous to the first photoisomerization, the major CD band decreased to $\Delta\varepsilon$ −5.7 (λ_{max} = 287 nm). ^{1}H NMR analysis clearly showed the formation of the *trans*-isomer as the characteristic absorption of the methoxy-protons now shifts downfield from δ 3.04 to 3.89 ppm. Furthermore, the doublet signal of the upper half methyl-protons was shifted downfield from δ 1.60 to 1.77 ppm, again indicating the conformational change resulting in a pseudo-axial instead of a pseudo-equatorial orientation of the methyl group. In the aromatic region two signals clearly belonging to (3′*S*)-(*M*)-*trans*-**1′a** appeared at δ 6.68–6.73 (m, 1H) and 6.86 ppm (dd, J = 9.0, 3.0 Hz, 1H) (all other signals overlap).

From these data and the CD spectrum at photoequilibrium the CD spectrum of pure (3′*S*)-(*M*)-*trans*-**1′a** could be calculated (Fig. 6) and again the pseudoenantiomeric relationship of (3′*S*)-(*M*)-*trans*-**1′a** and (3′*S*)-(*P*)-*cis*-**1b** is clearly visible. Heating this sample to 55 °C induced the helix inversion equilibrium (3′*S*)-(*M*)-*trans*-**1′a** ⇆ (3′*S*)-(*P*)-*trans*-**1a**. It should be noted that simultaneously again the thermal isomerization of (3′*S*)-(*P*)-*cis*-**1b** was induced. These thermal processes were again monitored by CD spectroscopy (Fig. 7).

Thermodynamic parameters of compound 1. The determination of thermodynamic parameters in the case of compound **1** was complicated compared to previous motor systems due to the fact that both thermal helix inversion steps are reversible under the experimental conditions used. Because of this the kinetic data obtained from the thermal helix inversion are the result of two thermal equilibria, *i.e.* two equilibrium constants with in total four reaction rates. The individual thermal equilibria are presented in Scheme 5. For both equilibria the energetically downhill forward helix inversion rate was denoted rate constant k_1 and the energetically uphill backward helix inversion k_2 and these two rate constants are related through the equilibrium constant ($K = k_1/k_2$). Modeling of the processes gave a good fit with the observed curves from CD measurement for both samples studied (Fig. 7).

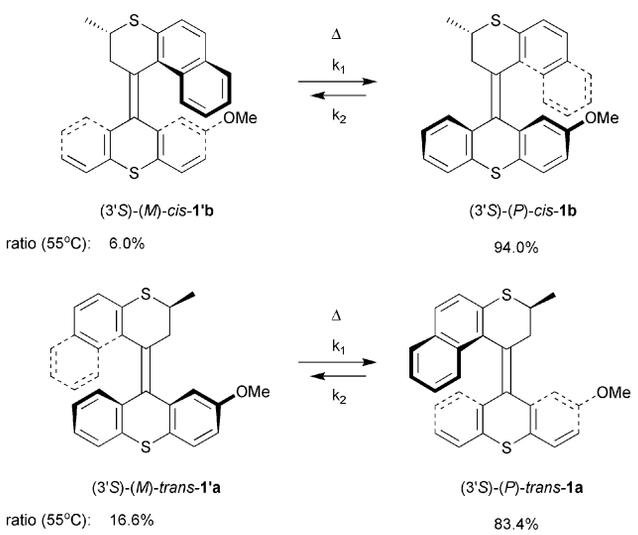

Scheme 5 Thermal helix inversion pathways for compound **1**.

The k-values thus obtained for *cis*-**1b** were $k_1 = 1.42 \times 10^{-5}$ s^{-1} and $k_2 = 9.08 \times 10^{-7}$ s^{-1}; the values obtained for *trans*-**1a** were $k_1 = 2.71 \times 10^{-5}$ s^{-1} and $k_2 = 5.41 \times 10^{-6}$ s^{-1} both at 55 °C. The respective Gibbs free energy of activation for the four different pathways gives an indication of the relative stability of the four isomers. At 55 °C, the *cis*-isomers ($\Delta G^{\ddagger}_{55\,°C\ (cis\text{-}\mathbf{1'b} \longrightarrow cis\text{-}\mathbf{1b})}$ = 111.03 kJ mol^{-1} and $\Delta G^{\ddagger}_{55\,°C\ (cis\text{-}\mathbf{1b} \longrightarrow cis\text{-}\mathbf{1'b})}$ = 118.54 kJ mol^{-1}) have a higher energy barrier for helix inversion compared to the *trans*-isomers ($\Delta G^{\ddagger}_{55\,°C\ (trans\text{-}\mathbf{1'a} \longrightarrow trans\text{-}\mathbf{1a})}$ = 109.27 kJ mol^{-1} and $\Delta G^{\ddagger}_{55\,°C\ (trans\text{-}\mathbf{1a} \longrightarrow trans\text{-}\mathbf{1'a})}$ = 113.67 kJ mol^{-1}). Surprisingly, the barriers for all thermal helix inversion were consider-

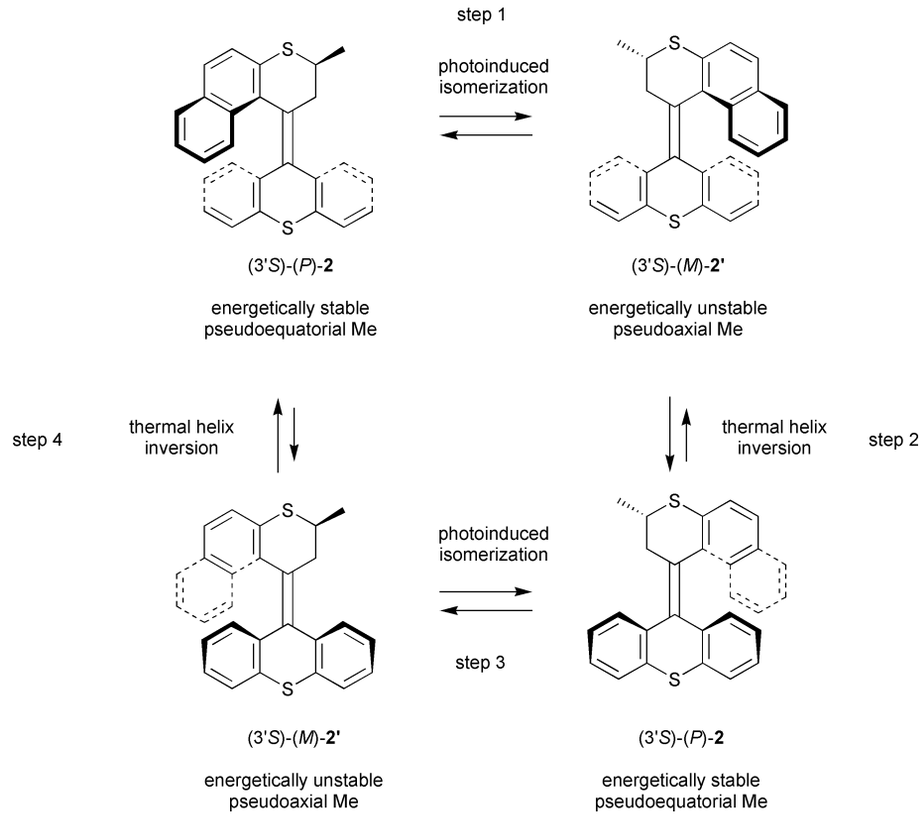

Scheme 6 Photochemical and thermal isomerization steps of newly designed sterically overcrowded alkene **2**.

ably higher than anticipated. A comparison of the barriers determined for compound **1** with the barrier of $\Delta G^{\ddagger}_{55\,^{\circ}C}$ = 101.37 kJ mol^{-1} determined for the second-generation motor, with a methoxy-substituent on both sides of the stator half of the molecule (Fig. 1B $R_1 = R_2 =$ OMe) can be made.[30] Much to our surprise, shifting the methyl substituent in the upper (rotor) part away from the fjord region resulted in a higher barrier and therefore slower rotation. Apparently in the case of compound **1**, energy barriers are not only influenced by steric factors but probably ground-state distortions also play a significant role.

Concerning the direction of rotation of 1. The observed ratios of stable and unstable forms are true Boltzmann distributions between the states. These thermal helix inversions will not be unidirectional processes at any temperature. Therefore, in case of compound **1**, we cannot speak of a truly unidirectionality rotating motor, *i.e.* a motor where the rotor part rotates exclusively in a clockwise direction relative to the stator part. Nevertheless, in all the discrete four steps of the intramolecular rotary process there is a preference for the direction that will lead to clockwise rotation in case of (3′*S*)-(*P*)-*trans*-**1a** (or counterclockwise rotation for (3′*R*)-(*M*)-*trans*-**1a**). Especially the first thermal helix inversion step (step 2 in Scheme 3) shows a substantial preference for the forward (energetically downhill) process. Therefore in the sense of a ratchet type rotary motor the present system qualifies.

Considering a molecular motor at work one should consider continuous rotation. Continuous rotation in this molecular system can be achieved by a continuous input of both photon energy (photoisomerization) and kinetic energy (thermal helix inversion) since all four isomerization steps will simultaneously take place under these conditions. It is a realistic assumption that the thermal helix inversions will be the rate determining steps, although light intensity and temperature are important parameters in this context. For the experiments described here, for which a 180 W Hg lamp with a $\lambda \geq 280$ nm Pyrex cut-off filter was used for photoirradiation and thermal helix inversion was investigated at a temperature of 55 °C, this assumption seems valid. Under continuous heating and irradiation, for both clockwise and counterclockwise rotation, the thermal helix inversion of the *cis*-isomers will be rate determining (since the barriers for helix inversion of *cis*-**1b** in both the forward (111.03 kJ mol^{-1}) and backwards direction (118.54 kJ mol^{-1}) are higher than the barriers for the helix inversion of *trans*-**1a** (109.27 and 113.67 kJ mol^{-1}, respectively). The rate constant of the forward clockwise rotation then equals the rate constant for the rate determining (*M*)-*cis*-**1′b** to (*P*)-*cis*-**1b** helix inversion (1.41×10^{-5} s^{-1}) and the rate constant of the backwards counterclockwise rotation equals the rate constant for the reverse (*P*)-*cis*-**1b** to (*M*)-*cis*-**1′b** helix inversion (9.02×10^{-7} s^{-1}). These values give the ratio of molecules rotating in either direction, 94% of all molecular motors will rotate in the anticipated clockwise direction and 6% rotate in the opposite counterclockwise direction (which is by definition the same as the thermal ratio for the helix inversion of *cis*-**1b**). This ratio is expected to be independent of temperature as long as the thermal steps remain rate determining.

Photochemical and thermal behavior of unsubstituted motor 2. Compound **2** is a simplified version of motor **1** with a symmetrical lower half. For this compound identical behavior was expected as found for **1**, the envisioned rotary cycle is depicted in Scheme 6. Although, due to the symmetric lower half, only two (3′*S*)-isomers exist, a four-step cycle is used to illustrate the overall rotary process (*cf.* Scheme 4). Starting from stable (3′*S*)-(*P*)-**2**, irradiation will result in the formation of energetically unfavorable (3′*S*)-(*M*)-**2′** (step 1). Upon thermal helix inversion stable (3′*S*)-(*P*)-**2** is formed again (step 2). A second irradiation (step 3) and heating step (step 4), identical to step 1 and 2, will result again in a total 360° rotation of the upper half of the molecule with respect to the lower half.

Indeed, for compound **2** all properties were very similar to those of compound **1**. CD and UV spectra of the two enantiomerically pure isomers, energetically stable (3′*S*)-(*P*)-**2** and energetically less stable (3′*S*)-(*M*)-**2′**, obtained after chiral separation of a photostationary mixture of both isomers are

depicted in Fig. 8. Analogous to the experiments described for compound **1**, the photochemical and thermal steps of the proposed four state intramolecular rotation were examined using UV-Vis, CD and NMR spectroscopy in chloroform ($CHCl_3$ and $CDCl_3$) solution. The CD spectrum of (3′*S*)-(*P*)-**2** and (3′*S*)-(*M*)-**2′** clearly indicate the pseudoenantiomeric relation.

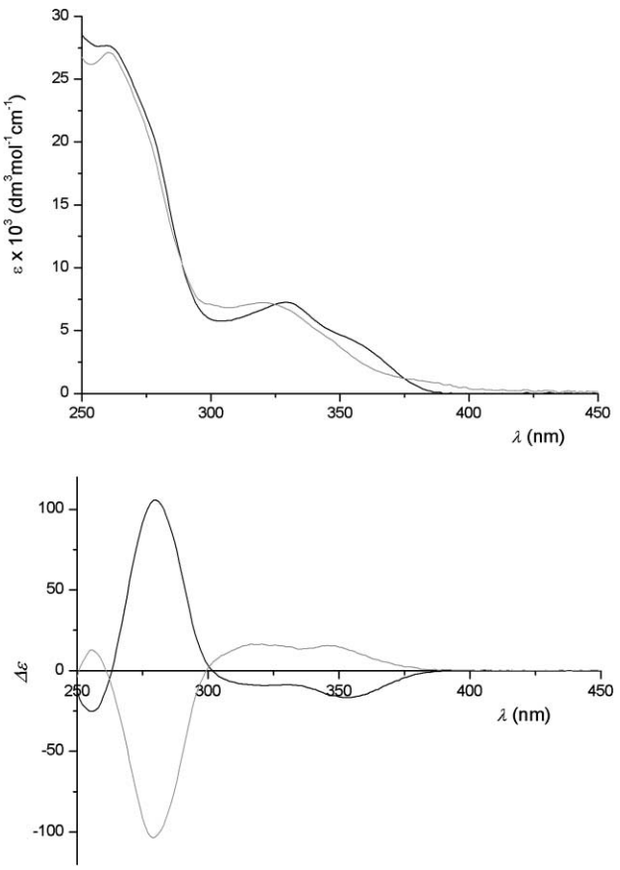

Fig. 8 UV (top) and CD (bottom) spectra of (3′*S*)-(*P*)-**2** (black) and (3′*S*)-(*M*)-**2′** (gray).

Irradiation of a sample of enantiomerically pure (3′*S*)-(*P*)-**2** in chloroform at $\lambda \geq 280$ nm, resulted in a photostationary state consisting of 53.5% (3′*S*)-(*M*)-**2′** and 46.5% (3′*S*)-(*P*)-**2** (as determined with ^{1}H NMR and CD spectroscopy). The isomer ratio is comparable to that of methoxy-substituted motor **1**. Analogues to the results obtained with compound **1**, ^{1}H NMR analysis showed a downfield shift of the doublet of the upper half methyl protons of **2** from δ 1.55 to 1.77 ppm indicating a pseudo-equatorial to pseudo-axial conformational change (all aromatic signals strongly overlap). The major CD band inverted sign and decreased substantially from $\Delta\varepsilon$ +105.8 (λ_{max} = 280 nm) to $\Delta\varepsilon$ −7.0 (λ_{max} = 277 nm).

Heating this sample at 55 °C resulted in a thermal equilibrium consisting of still 23.0% of (3′*S*)-(*M*)-**2′** and 77.0% of (3′*S*)-(*P*)-**2**. A mixture of (3′*S*)-(*M*)-**2′** and (3′*S*)-(*P*)-**2** with a similar ratio was obtained starting from either a solution of pure (3′*S*)-(*P*)-**2** or (3′*S*)-(*M*)-**2′**. The major CD band reflected the diastereomeric excess of (3′*S*)-(*P*)-**2** ($\Delta\varepsilon$ +57.8 (λ_{max} = 280 nm)). Again after thermal helix inversion a substantial amount of the energetically unfavorable isomer is present. The rate constants of the forward (**2′** ⟶ **2**) thermal helix inversion and the reverse pathway were determined by CD spectroscopy to be 5.01×10^{-5} s^{-1} and 1.50×10^{-5} s^{-1}, respectively at 55 °C. Both values are of the same order of magnitude as found for the substituted compound **1**. The Gibbs free energy barriers ($\Delta G^{\ddagger}_{55\,°C}$) are 107.86 kJ mol^{-1} for the energetically downhill (3′*S*)-(*M*)-**2′** to (3′*S*)-(*P*)-**2** helix inversion and 110.17 kJ mol^{-1} for the energetically uphill (3′*S*)-(*P*)-**2** to (3′*S*)-(*M*)-**2′** helix inversion at this temperature. A similar calculation as for **1** (*vide supra*) shows that for **2**, under conditions of continuous irradiation and heating at 55 °C (again under the assumption that the thermal helix inversions are the rate determining steps), 77% of the molecules will rotate in a clockwise fashion and 23% of the molecules will rotate in a counterclockwise fashion.

Conclusions

In the design of light-driven unidirectional molecular motors, the position and orientation of the methyl substituent at the stereogenic center were anticipated to be crucial parameters governing unidirectional rotation. The methyl substituent in the rotor part of the molecule was shifted one position away from the sterically demanding fjord region. In contrast to previous systems there is a preference for the methyl substituent to adopt a pseudo-equatorial orientation but again the methyl substituent has a preferred *anti*-orientation with respect to the lower (stator) half aromatic moiety. This new type of compound is still able to function as a molecular motor, albeit not with full unidirectionality. For the (3′*S*)-isomers of both the methoxy-substituted compound **1** and the unsubstituted variant **2**, there is a preferential clockwise rotation of one half of the molecule under the influence of light and heat. This preferential direction of rotation still sets this system apart from random Brownian motion.

An anticipated advantage of these new systems was that upon shifting the methyl substituent away from the sterically demanding fjord region barriers for thermal helix inversion would be lowered without severely distorting the ground state. Much to our surprise, comparing the energy barriers determined for these new motor molecules at 55 °C (ranging from $\Delta G^{\ddagger}_{55\,°C\ (\mathbf{2'} \longrightarrow \mathbf{2})}$ = 106.89 kJ mol^{-1} to $\Delta G^{\ddagger}_{55\,°C\ (\textit{cis}\text{-}\mathbf{1b} \longrightarrow \textit{cis}\text{-}\mathbf{1'b})}$ = 118.55 kJ mol^{-1}) with the values for the molecular motors with the methyl substituent at the 2′-position at the same temperature ($\Delta G^{\ddagger}_{(\text{stable} \longrightarrow \text{unstable})}$= 106.18 kJ mol^{-1} for the unsubstituted second-generation motor (Fig. 1B, $R_1 = R_2 = H$)) immediately shows that the effect of shifting the methyl substituent on the energy barrier is negligible. Even a slight increase in the barrier is observed which might be attributed to small differences in the ground or transition state conformations of the different compounds. Moreover, by shifting a single methyl substituent one position away from the fjord region of our molecular motors we are approaching the limits of the design. Compared to the first and second-generation molecular motors, which showed full unidirectionality, in the present cases only preferential rotation in one direction is found.

Although the experimental results show that the barriers for thermal helix inversion are not only governed by steric factors, increasing the size of the substituent next to the stereogenic center from a methyl to *e.g.* an isopropyl-group might prevent undesired energetically uphill thermal helix inversion and only influence the thermal barriers to a small extent. This could result in a third-generation of unidirectionally rotating molecular motors. These findings provide important guidelines for the construction of future generations of light-driven molecular motors.

Experimental

General procedure

^{1}H NMR spectra were recorded on a Varian Gemini-200 (200 MHz) or a Varian VXR-300 (300 MHz). ^{13}C NMR spectra were recorded on a Varian Gemini-200 (50 MHz) or a Varian VXR-300 (75 MHz). Chemical shifts are denoted in δ-unit (ppm) relative to $CDCl_3$ (δ 7.26 ppm). The splitting patterns are designated as follows: s (singlet), d (doublet), t (triplet), q (quartet), m (multiplet) and b (broad) for ^{1}H NMR. For ^{13}C NMR the carbon atoms are assigned as q (primary carbon), t (secondary carbon), d (tertiary carbon) and s (quaternary

carbon). CD spectra were recorded on a JASCO J-715 spectropolarimeter and UV measurements were performed on a Hewlett-Packard HP 8453 FT Spectrophotometer using UVASOL grade solvents (Merck). MS spectra were obtained with a Jeol JMS-600 spectrometer by Mr. A. Kieviet. Column chromatography was performed on silica gel (Aldrich 60, 230–400 mesh). HPLC analyses were performed on a Waters HPLC system equipped with a 600E solvent delivery system and a 996 Photodiode Array Detector. Preparative HPLC was performed on a preparative Gilson HPLC system consisting of a 231XL sampling injector, a 306 (10SC) pump, an 811C dynamic mixer, an 805 manometric module, with a 119 UV-VIS detector and a 202 fraction collector, using the (chiral) columns as indicated. Elution speed was 1 ml min^{-1}, unless stated otherwise. Solvents were distilled and dried before use, if necessary, by standard methods. Reagents and starting materials were used as obtained from Aldrich, Acros, Fluka or Merck.

Irradiation experiments

Irradiations were performed with an 150 W Oriel Xe-lamp attached to an Oriel monochromator or a 180 W Oriel Hg-lamp adapted with a suitable mercury line filter for 313, 365, 405 and 435 nm irradiations (typical bandwidth 10 nm). Photostationary states are ensured by monitoring composition changes with time by taking UV spectra at distinct intervals until no changes were observed. Ratios of the different isomers of **1** and **2** were determined by HPLC by monitoring at the isosbestic point or by NMR analysis. HPLC elution times and NMR details are denoted throughout the synthetic procedures. Thermal helix inversions were also monitored by CD spectroscopy employing a JASCO PFD-350S/350L Peltier type FDCD attachment with temperature control.

3-(2-Naphthylsulfanyl)butanenitrile 7

A mixture of 2-naphthalenethiol (3.2 g, 20 mmol), crotononitrile (1.34 g, 20 mmol) and piperidine (5 drops) was stirred for 45 min at room temperature. Triton B (40% solution in MeOH, 5 drops) and dioxane (2.5 ml) were added and the resulting mixture was heated at reflux for 24 h. The reaction mixture was dissolved in toluene (50 ml) and washed with water. Drying of the organic layer ($MgSO_4$) and subsequent removal of all volatiles gave a brown oil which was purified by column chromatography (SiO_2, heptane : EtOAc = 5 : 1, R_f = 0.34) yielding a colorless oil which solidified upon standing (4.16 g, 18 mmol, 91%, mp 28.5–29.5 °C); δ_H(300 MHz; $CDCl_3$) 1.48–1.51 (3 H, d, *J* 7.0), 2.37–2.64 (2 H, m), 3.49–3.55 (1 H, m), 7.49–7.55 (3 H, m), 7.79–7.85 (3 H, m), 7.96 (1H, s); δ_C (75.48 MHz; $CDCl_3$) 18.7 (q), 24.0 (t), 38.1 (d), 116.1 (s), 125.4 (d), 125.5 (d), 126.3 (d), 126.4 (d), 127.6 (d), 128.6 (s), 128.7 (d), 131.1 (d), 131.3 (s), 132.2 (s); *m*/*z* (EI) 227 (M^+, 100%), 187 (83), 160 (40), 115 (50); HRMS (EI): calcd. for $C_{14}H_{13}NS$: 227.0769, found 227.0777.

3-Methyl-2,3-dihydro-1*H*-benzo[*f*]thiochromen-1-one 8

To mechanically stirred PPA (100 mL) at 60 °C was added nitrile **7** (5.76 g, 25 mmol). The temperature was raised to 110 °C and stirring was continued for 3 h. The mixture was poured onto ice and left to stand overnight. The slightly yellow precipitate formed was isolated by filtration, after which it was purified by column chromatography (SiO_2, pentane : EtOAc = 10 : 1, R_f = 0.31), giving the ketone as a slightly yellow solid (4.89 g, 21 mmol, 86%, mp 55–56 °C); δ_H(300 MHz; $CDCl_3$) 1.47–1.50 (3 H, d, *J* 6.8), 2.85–2.98 (1 H, dd, *J* 15.4 and 11.5), 3.10–3.19 (1 H, dd, *J* 15.4 and 3.4), 3.66–3.77 (1 H, m), 7.24–7.28 (1 H, d, *J* 8.8), 7.40–7.48 (1 H, m), 7.56–7.64 (1 H, m), 7.72–7.81 (2H, m), 9.17–9.22 (1 H, d, *J* 8.8); δ_C(75.48 MHz; $CDCl_3$) 20.8 (q), 36.6 (d), 49.8 (t), 124.2 (s), 125.7 (d), 126.1 (d), 126.4 (d), 129.0 (d), 129.7 (d), 132.1 (s), 132.8 (s), 134.2 (d), 145.3 (s), 197.2 (s); *m*/*z* (EI) 228 (M^+, 56%), 186 (100), 158 (28); HRMS (EI): calcd. for $C_{14}H_{12}OS$: 228.0609, found 228.0610.

3-Methyl-2,3-dihydro-1*H*-benzo[*f*]thiochromen-1-one hydrazone 3

Ketone **8** (4.9 g, 21 mmol) was dissolved in a mixture of ethanol (20 ml) and hydrazine monohydrate (5.2 g, 0.10 mol, 5 eq) and subsequently refluxed for 2 h. The solution was then cooled to −18 °C from which the desired hydrazone could be collected as slightly yellow crystals (3.8 g, 18 mmol, 74%, mp 120.5–121.5 °C); δ_H(300 MHz; $CDCl_3$) 1.48–1.50 (3 H, d, *J* 7.0), 2.66–2.75 (1 H, dd, *J* 16.5 and 11.4), 3.05–3.12 (1 H, dd, *J* 16.5 and 4.0), 3.30–3.37 (1 H, m), 5.52 (2 H, br s), 7.29–7.32 (1 H, d, *J* 8.4), 7.37–7.42 (1 H, m), 7.45–7.51 (1 H, m), 7.60–7.63 (1H, d, *J* 8.4), 7.73–7.75 (1 H, d, *J* 7.7), 8.68–8.71 (1 H, d, *J* 8.4); δ_C(50.32 MHz; $CDCl_3$) 19.9 (q), 37.0 (d), 38.2 (t), 124.9 (d), 126.3 (d), 126.4 (d), 126.5 (d), 127.8 (d), 127.9 (d), 129.3 (s), 131.2 (s), 132.9 (s), 134.7 (s), 145.9 (s); *m*/*z* (EI) 242 (M^+, 100%); HRMS (EI): calcd. for $C_{14}H_{14}N_2S$: 242.0878, found 242.0870.

Dispiro[2,3-dihydro-3-methyl-1*H*-naphtho[2,1-*b*]thiopyran-1,2′-thiirane-3′,9″-(2″-methoxy-9″*H*-thioxanthene)] 6

Under a nitrogen atmosphere, a solution of hydrazone **3** (300 mg 1.24 mmol) in dry dichloromethane (10 ml) was cooled to −10 °C, whereupon $MgSO_4$ (500 mg), Ag_2O (430 mg, 1.81 mmol) and a few drops of a saturated solution of KOH in methanol were added successively. After stirring for 30 min the solution turned bright red. The solution was then filtered and a solution of the thioketone **4** in dichloromethane was added until the red color had disappeared. After removal of the organic volatiles in the reaction mixture, the product was purified by recrystallization from ethanol, giving the episulfides **6** as slightly yellow needles (310 mg, 0.66 mmol, 53%). Since no separation of the four isomeric episulfides could be accomplished, the mixture was subjected to the next step; *m*/*z* (EI) = 470 (M^+, 61%), 438 (100), 227 (56); HRMS (EI): calcd. for $C_{28}H_{22}OS_3$: 470.0833, found: 470.0815.

2-Methoxy-9-(2′,3′-dihydro-2′-methyl-1′*H*-naphtho[2,1-*b*]-thiopyran-1′-ylidene)-9*H*-thioxanthene 1

A solution of the episulfides **6** (310 mg, 0.66 mmol) and PPh_3 (0.26 g, 1.0 mmol) in *p*-xylene (30 ml) was refluxed overnight. After evaporation of the solvent, the product was purified by column chromatography (SiO_2, toluene : heptane = 10 : 1, R_f = 0.39) followed by repeated recrystallizations from ethanol giving the *cis*-**1** as slightly yellow crystalline mixture of stable and unstable diastereoisomers *cis*-**1b** and *cis*-**1′b** (70 mg, 0.16 mmol), and *trans*-**2**, also as a mixture of stable and unstable diastereoisomers *trans*-**1a** and *trans*-**1′a** as white crystals (80 mg, 0.18 mmol), both in an approximate 10 : 1 ratio of stable : unstable isomers (^{1}H NMR). The combined yield was 52%. *m*/*z* (EI) = 438 (M^+, 100%). HMRS (EI): calcd. for $C_{28}H_{22}OS_2$: 438.1112, found: 438.1107.

***trans*-1a**. δ_H(300 MHz; $CDCl_3$) 1.60–1.62 (3 H, d, *J* 6.5), 2.07–2.15 (1 H, d, *J* 12.5), 3.64–3.70 (1 H, dd, *J* 12.5 and 6.2), 3.87 (3 H, s), 4.14–4.18 (1 H, m), 6.42–6.54 (2 H, m), 6.74–6.79 (1 H, m), 6.85–6.89 (1 H, m), 6.99–7.13 (3 H, m), 7.29–7.34 (2 H, m), 7.50–7.60 (4 H, m); δ_C(50.32 MHz, $CDCl_3$) 24.3 (q), 38.5 (t), 41.8 (d), 55.5 (q), 112.7 (d), 113.1 (d), 124.3 (d), 124.4 (d), 125.3 (d), 125.5 (d), 125.7 (d), 126.3 (d), 126.4 (d), 126.8 (s), 127.5 (d), 127.8 (d), 128.3 (d), 128.5 (s), 129.4 (d), 131.2 (s), 132.9 (s), 133.5 (s), 133.5 (s), 134.6 (s), 134.7 (s), 137.3 (s), 138.0 (s), 158.3 (s).

***cis*-1b**. δ_H(300 MHz; $CDCl_3$) 1.59–1.61 (3 H, d, *J* 6.6), 2.06–2.10 (1 H, dd, *J* 12.8 and 11.7), 3.04 (3 H, s), 3.50–3.56 (1 H, dd, *J* 12.8 and 6.2), 4.08–4.12 (1 H, m), 5.98–5.99 (1 H, d, *J* 2.9), 6.34–6.38 (1 H, dd, *J* 8.6 and 2.7), 6.99–7.04 (1 H, m), 7.10–7.63 (10 H, m); δ_C(75.48 MHz; $CDCl_3$) 24.4 (q), 38.4 (t), 41.9 (d),

54.9 (q), 113.5 (d) 114.7 (d), 124.36 (d), 124.44 (d), 125.2 (s), 125.5 (d), 125.85 (d), 126.95 (d), 126.8 (d), 127.1 (2 × d), 127.45 (d), 127.54 (d), 127.7 (d), 128.7 (s), 131.3 (s), 132.9 (s), 133.5 (s), 133.9 (s), 134.6 (s), 135.6 (s), 136.2 (s), 139.1 (s), 157.7 (s).

Resolution was performed by chiral HPLC using Chiralcel OD stationary phase and *n*-heptane : 2-propanol 99 : 1 as the eluent at 1 ml min^{-1}. For *trans*-**1**, the first eluted fraction (t = 6.53 min) contained both (3′*R*)-(*M*)-*trans*-**1a** and (3′*S*)-(*M*)-*trans*-**1′a** in a ratio of 10 : 1. The second fraction (t = 8.49 min) contained enantiomerically pure (3′*S*)-(*P*)-*trans*-**1a** and the third fraction (t = 9.62 min) contained enantiomerically pure (3′*R*)-(*P*)-*trans*-**1′a**. For *cis*-**1**, the first eluted fraction (t = 6.32 min) contained both (3′*R*)-(*M*)-*cis*-**1b** and (3′*S*)-(*M*)-*cis*-**1′b** in a ratio of 10 : 1. The second fraction (t = 8.06 min) was enantiomerically pure (3′*S*)-(*P*)-*cis*-**1b** and the third fraction (t = 9.03 min) enantiomerically pure (3′*R*)-(*P*)-*cis*-**1′b**. For both the *cis*- and the *trans*-isomers, the different stereoisomers were analyzed by CD spectroscopy where (*M*)- and (*P*)-helicity could be assigned by comparison with related sterically overcrowded alkenes.[25]

(3′*S*)-(*M*)-*trans*-**1′a**: UV/Vis: $\lambda_{max}(CHCl_3)$/nm 263 (ε/dm^3 mol^{-1} cm^{-1} 25807), 324 (7272), 341 (6631); CD: $\lambda_{max}(CHCl_3)$/nm 256 ($\Delta\varepsilon$ +14.2), 281 (−114.8), 320 (+19.7), 343 (+18.9). (3′*S*)-(*P*)-*trans*-**1a**: UV/Vis: $\lambda_{max}(CHCl_3)$/nm 260 (ε/dm^3 mol^{-1} cm^{-1} 32529), 334 (7562), 358 (6418); CD: $\lambda_{max}(CHCl_3)$/nm 254 ($\Delta\varepsilon$ −37.9), 281 (+136.5), 323 (−14.6), 356 (−20.9). (3′*S*)-(*M*)-*cis*-**1′b**: UV/Vis: $\lambda_{max}(CHCl_3)$/nm 272 (ε/dm^3 mol^{-1} cm^{-1} 26390), 320 (7849), 345 (6084); CD: λ_{max} ($CHCl_3$)/nm 255 ($\Delta\varepsilon$ +29.9), 279 (−110.2), 316 (+10.7), 348 (+14.2). (3′*S*)-(*P*)-*cis*-**1b**: UV/Vis: $\lambda_{max}(CHCl_3)$/nm 250 (ε/dm^3 mol^{-1} cm^{-1} 29366), 29 (26969), 327 (6911), 353 (5835); CD: λ_{max} ($CHCl_3$)/nm 254 ($\Delta\varepsilon$ −66.3), 280 (+115.7), 359 (−16.8).

Dispiro[2,3-dihydro-3-methyl-1*H*-naphtho[2,1-*b*]thiopyran-1,2′-thiirane-3′,9″-(9″*H*-thioxanthene)] 7

Following the procedure used for the synthesis of episulfides **6**, episulfides **7** were obtained from hydrazone **3** (300 mg 1.24 mmol) and thioketone **5**. After evaporation of the solvent, the product was purified by crystallization from ethanol, giving the episulfides as slightly green needles (273 mg, 0.62 mmol, 51%). Since no separation of the two episulfide isomers could be accomplished, the mixture was subjected to the next step; *m*/*z* (EI) = 440 (M^+, 65%), 408 (100), 197 (92); HRMS (EI): calcd. for $C_{27}H_{20}S_3$: 440.0727, found 440.0717.

9-(2′,3′-Dihydro-2′-methyl-1′*H*-naphtho[2,1-*b*]thiopyran-1′-ylidene)-9*H*-thioxanthene 2

A solution of episulfides **7** (240 mg, 0.55 mmol) and PPh_3 (150 mg, 0.57 mmol) was refluxed overnight in *p*-xylene (25 ml). After evaporation of the solvent the product was purified by column chromatography (SiO_2, hexane : EtOAc = 10 : 1, R_f = 0.30), followed by recrystallization from ethanol yielding the olefin as white needles as a racemic mixture of stable and unstable isomers **2** and **2′** in an approximate ratio of 10 : 1 (125 mg, 0.31 mmol, 56%).

2: δ_H(300 MHz; $CDCl_3$) 1.58–1.61 (3 H, d, *J* 6.6), 2.04–2.12 (1 H, dd, *J* 12.5 and 12.1), 3.55–3.61 (1 H, dd, *J* 12.5 and 6.0), 4.13–4.17 (1 H, m), 6.44–6.55 (2 H, m), 6.75–6.79 (1 H, m), 6.97–7.55 (1 H, m), 7.08–7.13 (1 H, m), 7.29–7.64 (m, 9H); δ_C(50.32 MHz; $CDCl_3$) 23.3 (q), 37.4 (t), 40.8 (d), 123.2 (d), 123.3 (d), 124.4 (d), 124.5 (d), 124.7 (d), 125.1 (d), 125.3 (2 × d), 125.8 (d), 126.1 (d), 126.4 (d), 126.5 (d), 126.8 (d), 127.5 (s), 128.4 (d), 130.1 (s), 131.9 (s), 132.3 (s), 132.7 (s), 132.9 (s), 133.7 (s), 134.6 (s), 134.8 (s), 137.0 (s); *m*/*z* (EI) = 408 (M^+, 100%); HRMS (EI): calcd. for $C_{27}H_{20}S_2$: 408.1006, found: 408.1001.

Resolution was performed by chiral HPLC using Chiralcel OD stationary phase and *n*-heptane : 2-propanol 99 : 1 as the eluent at 1 ml min^{-1}. The first eluted fraction (t = 5.57 min) contained both (3′*R*)-(*M*)-**2** and (3′*S*)-(*M*)-**2′** in a ratio of 10 : 1. The second fraction (t = 6.74 min) contained enantiomerically pure (3′*S*)-(*P*)-**2** and the third fraction (t = 7.87 min) contained enantiomerically pure (3′*R*)-(*P*)-**2′**. The different stereoisomers were analyzed by CD spectroscopy where (*M*)- and (*P*)-helicity could be assigned by comparison with related sterically overcrowded alkenes.[25]

(3′*S*)-(*M*)-**2′**: UV/Vis: $\lambda_{max}(CHCl_3)$/nm 261 (ε/dm^3 mol^{-1} cm^{-1} 27123), 319 (7221), 382 (1004); CD: λ_{max} ($CHCl_3$)/nm 255 ($\Delta\varepsilon$ +12.7), 279 (−103.7), 317 (+16.4), 345 (+15.5). (3′*S*)-(*P*)-**2**: UV/Vis: $\lambda_{max}(CHCl_3)$/nm 241 (ε/dm^3 mol^{-1} cm^{-1} 32828), 260 (27663), 329 (7256), 360 (3674); CD: λ_{max} ($CHCl_3$)/nm 255 ($\Delta\varepsilon$ −25.2), 280 (+105.8), 322 (−9.4), 353 (−16.8).

Crystal structure determination of compound 2

Crystal data. $C_{27}H_{20}S_2$, M = 408.59, monoclinic, a = 8.827(2), b = 21.647(4), c = 11.075(2) Å, U = 2080.8(7) Å^3, T = 293(1) K, space group $P2_1/n$ (no. 14), Z = 4, μ = 2.670 cm^{-1}, 14823 reflections measured, 3673 unique (R_{int} = 0.0379) which were used in all calculations. The final $wR(F^2)$ was 0.1342 (all data). ‡

‡ CCDC reference number 231703. See http://www.rsc.org/suppdata/ob/b4/b402222j/ for crystallographic data in.cif or other electronic format.

References

1 (*a*) *Sci. Am.* Special Issue: *Nanotech: The Science of Small Gets Down to Business*, September 2001; (*b*) R. P. Feynman in *Miniaturization*, ed. H. D. Gilbert, Reinhold, New York, 1961; (*c*) V. Balzani, M. Venturi and A. Credi, *Molecular Devices and Machines – A Journey into the Nanoworld*, Wiley-VCH, Weinheim, 2003.

2 B. L. Feringa, N. Koumura, R. A. van Delden and M. K. J. ter Wiel, *Appl. Phys. A*, 2002, **75**, 301–308.

3 (*a*) B. L. Feringa, R. A. van Delden, N. Koumura and E. M. Geertsema, *Chem. Rev*, 2000, **100**, 1789–1816; (*b*) *Molecular Switches*, ed. B. L. Feringa, Wiley, Weinheim, 2001.

4 T. R. Kelly, M. C. Bowyer, K. V. Bhaskar, D. Bebbington, A. Garcia, F. R. Lang, M. H. Kim and M. P. Jette, *J. Am. Chem. Soc.*, 1994, **116**, 3657–3658.

5 (*a*) A. M. Stevens and C. J. Richards, *Tetrahedron. Lett.*, 1997, **38**, 7805–7808; (*b*) J. Clayden and J. H. Pink, *Angew. Chem., Int. Ed. Engl.*, 1998, **37**, 1937–1939; (*c*) W. D. Hounshell, C. A. Johnson, A. Guenzi, F. Cozzi and K. Mislow, *Proc. Natl. Acad. Sci.*, 1980, **77**, 6961–6964; (*d*) F. Cozzi, A. Guenzi, C. A. Johnson and K. Mislow, *J. Am. Chem. Soc.*, 1981, **103**, 957–958; (*e*) Y. Kawada and H. Iwamura, *J. Org. Chem.*, 1980, **45**, 2547–2548; (*f*) Y. Kawada and H. Iwamura, *J. Am. Chem. Soc.*, 1981, **103**, 958–960.

6 T. C. Bedard and J. S. Moore, *J. Am. Chem. Soc.*, 1995, **117**, 10662–10671.

7 T. Muraoka, K. Kinbara, Y. Kobayashi and T. Aida, *J. Am. Chem. Soc.*, 2003, **125**, 5612–5613.

8 K. Tashiro, K. Konishi and T. Aida, *J. Am. Chem. Soc.*, 2000, **122**, 7921–7926.

9 M. C. Jiménez, C. Dietrich-Buchecker and J.-P. Sauvage, *Angew. Chem., Int. Ed.*, 2000, **39**, 3284–3287.

10 (*a*) J. P. Abrahams, A. G. W. Leslie, R. Lutter and J. E. Walker, *Nature*, 1994, **370**, 621–628; (*b*) H. Noji, M. Yasuda and K. Kinosita Jr., *Nature*, 1997, **386**, 299–302; (*c*) Special Issue *Science*: *Movement: Molecular to Robotic*, 2000, **288**, pp. 79–106.

11 See for example: *Molecular Motors*, ed. M. Schliwa, Wiley-VCH, Weinheim, 2003.

12 *Molecular Machines and Motors*, ed. J.-P. Sauvage, *Structure and Bonding*, Vol. 99, Springer, Berlin, 2001; (*a*) V. Balzani, M. Venturi and A. Credi, *Molecular Devices and Machines – A Journey into the Nanoworld*, Wiley-VCH, Weinheim, 2003.

13 (*a*) L. Zelikovich, J. Libman and A. Shanzer, *Nature*, 2002, **374**, 790–792; (*b*) V. Amendola, L. Fabbrizzi, C. Mangano and P. Pallavicini, *Acc. Chem. Res.*, 2001, **34**, 488–493.

14 For reviews see, for example: (*a*) V. Balzani, A. Credi, M. Raymo and J. F. Stoddard, *Angew. Chem., Int. Ed.*, 2000, **39**, 3349–3391; (*b*) A. R. Pease, J. O. Jeppesen, J. F. Stoddart, Y. Luo, C. P. Collier and J. R. Heath, *Acc. Chem. Res.*, 2001, **34**, 433–444; (*c*) R. Ballardini, V. Balzani, A. Credi, M. T. Gandolfi and M. Venturi, *Acc. Chem. Res.*, 2001, **34**, 445–455; (*d*) C. A. Schalley, K. Beizai and F. Vögtle, *Acc. Chem. Res.*, 2001, **34**, 465–476; (*e*) J.-P.

Collin, C. Dietrich-Buchecker, P. Gaviña, M. C. Jiminez-Molero and J.-P. Sauvage, *Acc. Chem. Res.*, 2001, **34**, 477–487.
15 T. R. Kelly, H. De Silva and R. A. Silva, *Nature*, 1999, **401**, 150–152.
16 N. Koumura, R. W. J. Zijlstra, R. A. van Delden, N. Harada and B. L. Feringa, *Nature*, 1999, **401**, 152–155.
17 For recent examples of molecular motors: (*a*) D. A. Leigh, J. K. Y. Wong, F. Dehez and F. Zerbetto, *Nature*, 2003, **424**, 174–179; (*b*) P. Thordarson, E. J. A. Bijsterveld, A. E. Rowan and R. J. M. Nolte, *Nature*, 2003, **424**, 915–918.
18 R. A. van Delden, M. K. J. ter Wiel, N. Koumura and B. L. Feringa, in *Molecular Motors*, ed. M. Schliwa, Wiley-VCH, Weinheim, 2003, Chapter 23, pp. 559–577.
19 B. L. Feringa, R. A. van Delden and M. K. J. ter Wiel in *Molecular Switches*, ed. B. L. Feringa, Wiley-VCH, Weinheim, 2001, Chapter 5, pp. 123–163.
20 B. L. Feringa, N. P. M. Huck and H. A. van Doren, *J. Am. Chem. Soc.*, 1995, **117**, 9929–9930.
21 R. A. van Delden, M. B. van Gelder, N. P. M. Huck and B. L. Feringa, *Adv. Funct. Mater.*, 2003, **13**, 319.
22 R. A. van Delden, N. Koumura, N. Harada and B. L. Feringa, *Proc. Nat. Acad. Sci.*, 2002, **99**, 4945–4949.
23 T. Hugel, N. B. Holland, A. Cattani, L. Moroder, M. Seitz and H. E. Gaub, *Science*, 2002, **296**, 1103–1106.
24 N. Koumura, E. M. Geertsema, A. Meetsma and B. L. Feringa, *J. Am. Chem. Soc.*, 2000, **122**, 12005–12006.
25 N. Koumura, E. M. Geertsema, M. B. van Gelder, A. Meetsma and B. L. Feringa, *J. Am. Chem. Soc.*, 2002, **124**, 5037–5051.
26 E. M. Geertsema, N. Koumura, M. K. J. ter Wiel, A. Meetsma and B. L. Feringa, *Chem. Commun.*, 2002, 2962–2963.
27 (*a*) D. H. R. Barton and B. J. Willis, *J. Chem. Soc., Chem. Commun.*, 1970, 1225–1226; (*b*) R. M. Kellogg, J. Buter and S. Wassenaar, *J. Org. Chem.*, 1972, **37**, 4045–4060.
28 The numbering of the atoms adopted in the X-ray structure is according to IUPAC rules, since this numbering is different from the numbering in the cif file‡ a conversion table is included in the Supporting Information†.
29 J. J. P. Stewart, MOPAC93-AM1, Fujitsu Ltd., Tokyo, Japan, 1993.
30 See supplementary material of reference 25.